High-order phonon anharmonicity in Yb-filled skutterudites

Hong-Jie Pang,[1] Hao Yu,[2,1] Wei-Jian Li,[3,1] Liu-Cheng Chen,[2,1] Peng-Fei Qiu,[4] Qing Peng,[2] and Xiao-Jia Chen[5,*]

[1]*Center for High Pressure Science and Technology Advanced Research, Shanghai 201203, China*

[2]*School of Science, Harbin Institute of Technology, Shenzhen 518055, China*

[3]*National Laboratory of Solid State Microstructures and School of Physics, Nanjing University, Nanjing 210093, China*

[4]*State Key Laboratory of High Performance Ceramics and Superfine Microstructure, Shanghai Institute of Ceramics, Chinese Academy of Sciences, Shanghai 200050, China*

[5]*Department of Physics and Texas Center for Superconductivity, University of Houston, Houston, Texas 77204, USA*

(Received 30 April 2023; revised 8 December 2023; accepted 3 January 2024; published 16 January 2024)

A study of the anharmonic phonon-scattering processes in Yb-filled $CoSb_3$ skutterudite with low lattice thermal conductivity is carried out by combining temperature-dependent Raman-scattering measurements and first-principles calculations. The softening of the phonon frequency reveals the phonon anharmonicity. The two selected phonon modes exhibit strong cubic and quartic anharmonicity. The calculated weighted phase space and scattering rates of three- and four-phonon scattering further support the anharmonicity. At high temperatures, four-phonon scattering dominates the phonon-scattering processes at low frequencies. Fermi resonances among low-frequency phonons provide strong four-phonon scattering, leading to low lattice thermal conductivity. This study provides insight into the nature of anharmonic processes in highly efficient Yb-filled skutterudites and demonstrates the important role of the high-order phonon-phonon interactions in lowering lattice thermal conductivity.

DOI: 10.1103/PhysRevB.109.045201

I. INTRODUCTION

Thermoelectric materials have attracted much attention for sustainable energy applications due to their ability to convert waste heat into useful electricity. High performance thermoelectric materials should have low lattice thermal conductivity and a high power factor [1–5]. Currently, the typical approaches are to optimize the electrical properties by optimizing the carrier concentration and band engineering or to reduce the lattice thermal conductivity by introducing various defects to scatter phonons [2]. The concept of "phonon-glass electron-crystal" (PGEC) proposed by Slack combines the low thermal conductivity of glass with the good electrical properties of crystal, which plays a key role in selecting thermoelectric materials [1]. As a representative of PGEC, filled skutterudite has a very low lattice thermal conductivity and a large power factor [6]. Filled skutterudites have a unique cagelike structure. Filling the vacancies in the cage with guest atoms can significantly reduce the lattice thermal conductivity without deteriorating the power factor [7–10]. Many efforts have been concentrated on understanding the relatively low lattice thermal conductivity in filled skutterudites. However, the mechanism that accurately reveals the lattice thermal conductivity in filled skutterudites remains controversial [11–21].

Several mechanisms have been proposed to explain the low lattice thermal conductivity in filled skutterudites. In the PGEC picture, the guest atoms are loosely bonded with the parent, just like "rattlers." The local vibrations of these rattlers provide an additional channel for phonon scattering, reducing the mean free path of phonons and thus the lattice thermal conductivity [11,12]. The PGEC picture has been considered for a long time as a mechanism for the low thermal conductivity in filled skutterudites. Surprisingly, a quasiharmonic coupling between the guest atoms and the host lattice in (La, Ce)Fe_4Sb_{12} has broken down this paradigm [13]. However, an independent vibration mode of the guest atom has been observed in Yb-filled skutterudite by time-of-flight inelastic neutron scattering measurements (INS) [14,15]. Meanwhile, the avoided crossing between the acoustic and low-frequency optic phonons found in $YbFe_4Sb_{12}$ and $LaFe_4Sb_{12}$ has also been proposed as a possible mechanism for the suppression of acoustic-phonon transport [16–18]. Furthermore, the low lattice thermal conductivity in filled skutterudite has also been suggested to be related to the lattice anharmonicity [19,20]. In our previous study, strong anharmonicity in Yb-filled skutterudite has been suggested from the large average Grüneisen parameter. And the strong anharmonicity is driven by the hybridization of the Yb-filled atom and the host framework [21]. Recently, four-phonon Fermi resonance has been discovered in the calculations of Yb-filled $FeSb_3$ skutterudite. Quartic anharmonicity in the phonon-scattering process significantly suppresses the thermal transport [22,23]. This motivates a comprehensive study of the phonon anharmonicity in filled skutterudites. Clearly, studies in this direction are still needed. The origin of the anharmonicity in filled skutterudites and the identification of the specific phonon-scattering processes remain to be examined. Therefore, investigations of phonon-scattering processes and phonon anharmonicity in

*xjchen@uh.edu

filled skutterudites are highly desired, in terms of both experiments and calculations.

Phonon-scattering processes determine the lattice thermal conductivity [24–30]. Information on phonon-scattering processes is crucial for understanding the mechanism of lattice thermal conductivity. A characteristic of anharmonicity is that the eigenfrequency varies with temperature [13]. The neutron scattering technique has been exclusively used to study the phonon density of states (PDOS) in filled skutterudites [11,13,14,18,19]. The Raman-scattering technique has access to some of the phonon branches at the Brillouin zone center [16,31,32]. Moreover, the Raman-scattering technique has a high resolution and no requirement on the sample size. It is a unique technique to detect the phonon vibrational information of thermoelectric materials at a wide temperature range [21,33–38]. The importance of the Raman-scattering technique in providing phonon information has recently been highlighted on filled skutterudites [39–43]. Importantly, the phonon anharmonicity can be investigated by the frequency shift or the change of the FWHM with temperature [33,34,37,44]. The filling atom induces an infrared active mode that is insensitive to Raman scattering. There are eight Raman-active modes in filled skutterudites, which are relatively large. Therefore it is necessary to study the anharmonicity and phonon-scattering processes in filled skutterudites by Raman scattering.

In this study we choose an efficient Yb-filled $CoSb_3$ skutterudite by using Raman-scattering measurements and first-principles calculations over a wide temperature range to reveal the phonon-scattering mechanism. The frequency shift and FWHM variation are obtained from temperature-dependent Raman-scattering measurements. The anharmonicity is evaluated by three- and four-phonon scattering processes. The scattering rates and weighted phase space are calculated to reveal the origin of the anharmonicity in detail. The combined experiments and calculations provide a comprehensive understanding of phonon-scattering processes and anharmonicity in filled skutterudites.

II. EXPERIMENTAL AND CALCULATION DETAILS

The sample was synthesized by a melt spinning and spark plasma sintering process. The detailed process can be found elsewhere [45]. The actual composition of the sample was determined by an energy-dispersive spectrometer (EDS, Oxford). The ambient-pressure structure of the sample was characterized using a RigakuD/MAX-2550PC diffractometer under Cu $K\alpha$ radiation with a wavelength of 1.5406 Å.

The thermal conductivity at low temperatures (2 K–300 K) was measured using the thermal transport option (TTO) of a physical property measurement system (PPMS, Quantum Design). At high temperatures (300 K–800 K) the thermal conductivity was estimated using a laser flash method on a Netzsch LFA457 instrument, with a Pyroceram standard.

The temperature-dependent Raman spectra were acquired through an excitation laser wavelength of 488 nm emitted by a sapphire laser (Coherent) [21]. The sample signal was recorded by a spectrometer (Princeton Instruments) coupled to a CCD. The laser power was below 2.5 mW to protect the sample from possible damage. The Raman-scattering measurements include two steps: low temperature (10 K–300 K) and high temperature (300 K–720 K). The low-temperature measurements were performed in a liquid helium continuous flowing cryostat. The temperature controller controls the sample temperature through a heater and a platinum resistance temperature detector with a typical accuracy of ±0.5 K. The high-temperature measurements were performed in a controlled atmosphere furnace. The temperature of the sample on the heating platform is controlled by setting the heating power. High-laser-transparency quartz windows were integrated into the furnace to avoid signal interference. A protective gas containing 97% argon and 3% hydrogen was continuously purged to avoid oxidation of the sample. Raman spectra were collected at 10-K intervals.

All the calculations were performed based on density-functional theory (DFT) with the projector-augmented-wave (PAW) method and a Perdew-Burke-Ernzerhof–type generalized gradient approximation (GGA) [46]. The geometry optimization of the unit cell was done with a $5 \times 5 \times 5$ k-point grid in the Vienna *ab initio* simulation package (VASP) [47,48]. The plane-wave basis was set with a cutoff energy of 520 eV. The lattice constants and ionic coordinates were relaxed to find the most stable states for $YbCo_4Sb_{12}$. Considering the low thermal expansion of the Yb-filled skutterudite [49], the effect of thermal expansion on thermal properties was not taken into account in the current calculation. The weighted phase space and scattering rates were determined from the harmonic, third- and fourth-order interatomic force constants (IFCs). The harmonic IFCs were calculated using a $2 \times 2 \times 2$ supercell implemented in the PHONOPY package [50]. The calculations of the third- and fourth-order IFCs were performed using the THIRDORDER and FOURTHORDER packages of the SHENGBTE [29,51], respectively. The $2 \times 2 \times 2$ and $1 \times 1 \times 1$ supercells were applied, respectively. This choice was based on the previous studies and the limitations of resources available to us [17,21,29]. The weighted phase space and scattering rates were obtained by employing ShengBTE with a q grid of $6 \times 6 \times 6$ and a scalebroad of 0.1. The convergence of the results was examined concerning the parameters employed in the calculations.

III. RESULTS AND DISCUSSION

A. Filled skutterudite with low lattice thermal conductivity

Filled skutterudite has a body-centered cubic crystal structure with space group $Im\bar{3}$, as shown in Fig. 1(a). The general formula for filled skutterudite is RM_4X_{12}, where $M =$ Co, Rh, or Ir, $X =$ P, As, or Sb, and R is a rare earth element [1]. The M and X atoms form eight octahedra with shared corners in a unit cell. The M atoms are located at the center of the octahedra and the X atoms are at the corners. These octahedra are tilted so that the X atoms form planar rectangular X_4 rings. The structural vacancies located at the corners and body center of the unit cell can be occupied by R atoms. The R atom with a small radius rattles in oversized cages within the skutterudite framework, reducing the lattice thermal conductivity of filled skutterudites.

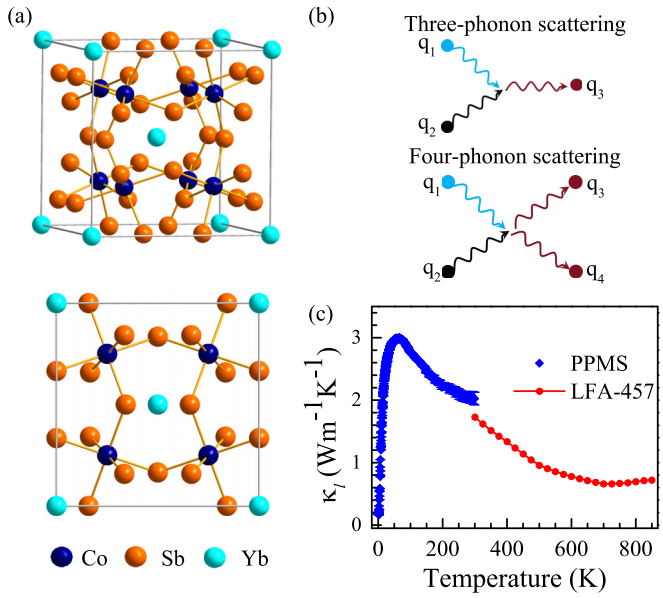

FIG. 1. (a) The crystal structure of Yb-filled $CoSb_3$ skutterudite from the side view (upper panel) and the top view (lower panel). (b) Schematic examples for three-phonon scattering (combination process) and four-phonon scattering (redistribution process). (c) Temperature dependence of the lattice thermal conductivity of $Yb_{0.3}Co_4Sb_{12}$ measured by a physical properties measurement system (PPMS) and a laser flash method (Netzsch, LFA 457).

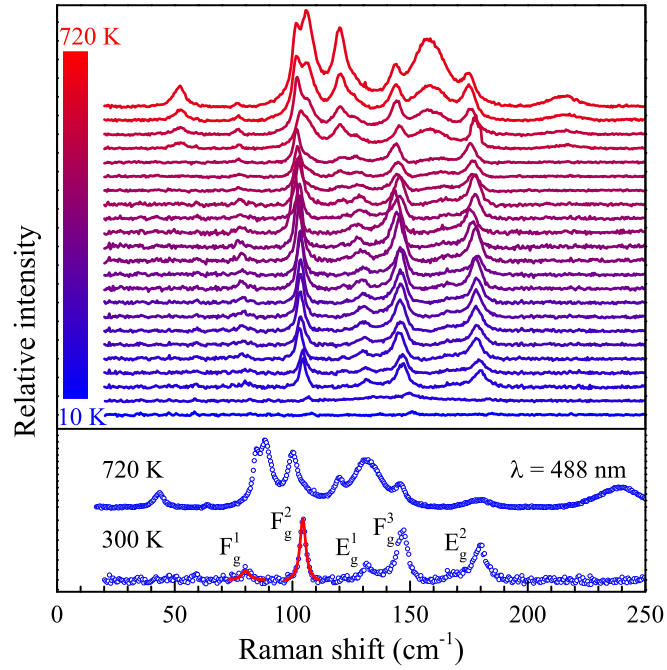

FIG. 2. Raman spectra of $Yb_{0.3}Co_4Sb_{12}$ at various temperatures from 10 to 720 K (upper panel). The lower panel shows the representative Raman spectra at temperatures of 300 and 720 K. The open circles are the experimental data points, and the curves are the fitting results by using a single Lorentzian function for each mode.

Temperature-dependent lattice thermal conductivity of Yb-filled $CoSb_3$ skutterudite is demonstrated in Fig. 1(c). The discontinuity of the lattice thermal conductivity at 300 K is due to the different measurements used for high and low temperatures. Due to the different principles and measurement techniques employed by PPMS and laser flash analysis (LFA), they can yield slightly different thermal conductivity results. The increase of the lattice thermal conductivity with increasing temperature above 700 K may be attributed to the bipolar thermal conductivity, which is widely observed in narrow-band thermoelectric materials, such as Bi_2Te_3 and PbTe [52]. This could be a result of the significant excitation of charge carriers at high temperatures. The lattice thermal conductivity of $Yb_{0.3}Co_4Sb_{12}$ shows a λ-shaped trend with increasing temperature, reaching 1.7 $Wm^{-1}K^{-1}$ at 300 K and the minimum 0.7 $Wm^{-1}K^{-1}$ around 600 K. These values are smaller than those of other single-filled skutterudites and comparable to those of multielement-filled skutterudites [53]. Moreover, the lattice thermal conductivity of Yb-filled $CoSb_3$ skutterudite is comparable to many high-performance thermoelectric materials, such as SnSe, PbTe, $AgSbTe_2$, GeTe, and Zintl phases [53]. These thermoelectric materials have intrinsically low thermal conductivity due to large anharmonicity. Weak bonding and heavy elements induce large phonon anharmonicity, resulting in low lattice thermal conductivity. The filled atom is loosely bonded to the parent lattice, which favors phonon anharmonicity.

The anharmonic phonon-scattering processes include three-phonon, four-phonon, and higher-order phonon scattering [25]. Figure 1(b) illustrates the three- and four-phonon scattering processes. According to perturbation theory, the three-phonon scattering process could be one phonon splitting into two phonons or two phonons combing to create a new phonon. Compared with three-phonon scattering, four-phonon scattering involves more phonons and has splitting, redistribution, and combination processes [24]. Figure 1(b) shows the combination process of three-phonon scattering and the redistribution process of four-phonon scattering, respectively.

To further understand the phonon-scattering microscopic mechanism in filled skutterudites, we perform the temperature-dependent Raman-scattering measurements on Yb-filled $CoSb_3$ skutterudite.

B. Temperature-dependent Raman spectra

The temperature-dependent Raman spectra on $Yb_{0.3}Co_4Sb_{12}$ over a wide range from 10 to 720 K are shown in the upper panel of Fig. 2. According to group theory, 17 atoms in the primitive cell of $YbCo_4Sb_{12}$ give rise to 51 different phonon vibrational modes, including three acoustic-phonon modes and 48 optic-phonon modes. The contribution of optic-phonon modes to the lattice thermal conductivity is not negligible due to the number of optic-phonon modes. According to the irreducible representation, the optic-phonon modes can be denoted as $2A_g \oplus 2E_g \oplus 4F_g \oplus 2A_u \oplus 2E_u \oplus 8F_u$. The modes with A_g, E_g, and F_g symmetries are Raman active. There are eight Raman-active modes [43]. Following first-principles calculations [12], the observed phonon peaks in the lower panel of Fig. 2 are determined as $3F_g$, and $2E_g$, respectively. The phonon peaks of $Yb_{0.3}Co_4Sb_{12}$ are wider and the frequencies are lower than those of unfilled skutterudite

$CoSb_3$ [39,43], which is consistent with the theoretical calculations [12]. All the observed modes are the motions of Sb atoms. These results are consistent with the calculations of the projected density of states [12].

The evolution of the Raman spectra of $Yb_{0.3}Co_4Sb_{12}$ with temperature is shown in the upper panel of Fig. 2. With increasing temperature, the frequencies of all the detected Raman peaks exhibit softening, indicating phonon anharmonicity. And the broadening of the FWHMs implies short phonon lifetimes and high scattering rates. At higher temperatures we observed some new peaks, indicating changes in the lattice structure. Representative Raman spectra at temperatures of 300 and 720 K are shown in the lower panel of Fig. 2. The temperature-induced changes can be observed from the two Raman spectra. The temperature-dependent frequencies and FWHMs for each phonon mode were extracted by fitting the Raman spectra with Lorentzian functions.

C. Phonon anharmonicity

According to the Klemens-Hart-Aggarwal-Lax model, one phonon decays into two($\omega_0 \rightarrow \Sigma\omega_n$, $n = 1, 2$) or three ($\omega_0 \rightarrow \Sigma\omega_m$, $m = 1, 2, 3$) phonons [54,55]. The frequencies and linewidth can be expressed as functions of the cubic (three-phonon process) and quartic (four-phonon process) anharmonic terms [56]:

$$\omega_i(T) = \omega_{i0} + A\left(1 + \sum_{n=1}^{2} \frac{1}{e^{\hbar\omega_n/k_BT} - 1}\right) + B\left[1 + \sum_{m=1}^{3}\left(\frac{1}{e^{\hbar\omega_m/k_BT} - 1} + \frac{1}{(e^{\hbar\omega_m/k_BT} - 1)^2}\right)\right], \quad (1)$$

$$\Gamma_i(T) = \Gamma_{i0} + C\left(1 + \sum_{n=1}^{2} \frac{1}{e^{\hbar\omega_n/k_BT} - 1}\right) + D\left[1 + \sum_{m=1}^{3}\left(\frac{1}{e^{\hbar\omega_m/k_BT} - 1} + \frac{1}{(e^{\hbar\omega_m/k_BT} - 1)^2}\right)\right], \quad (2)$$

where $\hbar$ is the reduced Plank constant, k_B is the Boltzmann constant, ω_{i0} and Γ_{i0} are the phonon frequency and linewidth at 0 K, and ω_n and ω_m are the phonon frequencies involved in the three- and four-phonon scattering processes. A, B, C, and D are constants proportional to the strength of the three- and four-phonon scattering processes, respectively.

The frequency shift $\Delta\omega_i(T)_V$ corresponding to the thermal expansion is obtained as follows [57]:

$$\Delta\omega_i(T)_V = \omega_{i0}\left[\exp(-\gamma \int_0^T \alpha_V dT') - 1\right], \quad (3)$$

where γ is the Grüneisen parameter and α_V is the volume thermal expansion coefficient. For the studied Yb-filled $CoSb_3$ skutterudite, the γ values can be obtained from the experiments [21]. The available linear expansion coefficient α_l value is 8.17×10^{-6} K^{-1} [49]. The volume thermal expansion coefficient $\alpha_V = 3\alpha_l$ is used in the data fitting.

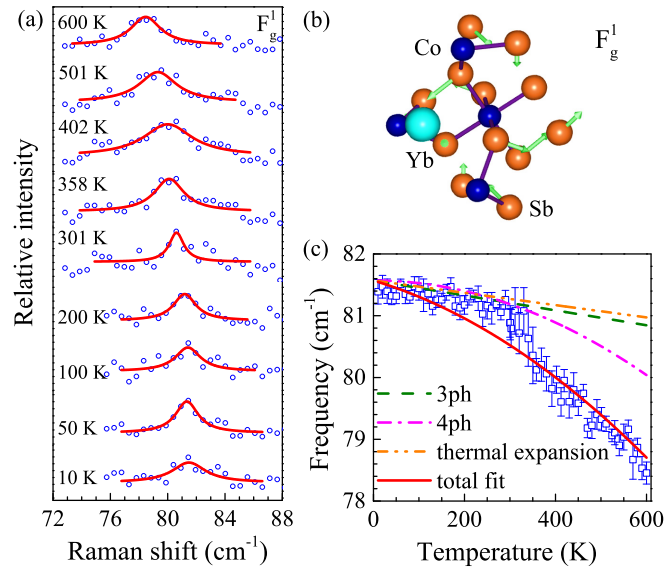

FIG. 3. (a) Raman spectra of the F_g^1 mode at various temperatures from 10 to 600 K. The open circles are the experimental data points and the curves are the fitting results by using a single Lorentzian function for the mode. (b) The vibration directions of the atoms for the F_g^1 mode. (c) Temperature dependence of the frequency of the F_g^1 mode. The red-solid line gives the theoretical fit using the processes of three- and four-phonon scattering and thermal expansion. The dashed lines describe the cubic and quartic terms of the anharmonicity and thermal expansion contributions, respectively.

Based on theoretical calculations, the corresponding phonon frequency for Yb filling is 42 cm^{-1} [10]. In addition, researchers have found two Einstein vibrational modes with corresponding frequencies of 40 and 100 cm^{-1} from the study of the specific heat of Yb-filled skutterudites $Yb_{0.2}Co_4Sb_{12}$. Meanwhile, the INS study has identified the two peaks in the PDOS at around 5 and 12.4 meV, consistent with the specific heat data [14]. Therefore we select the F_g^1 and F_g^2 modes, which are closest to the two Einstein modes in the Raman spectrum, to investigate the phonon anharmonicity in $Yb_{0.3}Co_4Sb_{12}$. Since the minimum of the lattice thermal conductivity is around 600 K, and the sample was damaged due to the laser heating effect above 640 K, we only fit the frequency and FWHM from 10 to 600 K.

The F_g^1 mode is a low-frequency optic-phonon mode and also the closest optic branch to the first Einstein mode. The assignment is illustrated in Fig. 3(b). The F_g^1 mode is due to the vibration of the Sb atoms, and it is a shear mode in the plane of the longer edge of the nearest Sb_4 ring. The phonon frequency for the F_g^1 mode is 80 cm^{-1} at 300 K, in agreement with previous studies [21], As for this vibrational mode, the Raman frequency corresponding to the parent skutterudite $CoSb_3$ is 87 cm^{-1}, and the frequencies corresponding to the filled skutterudites $LaFe_3CoSb_{12}$, $CeFe_3CoSb_{12}$, and $LaCeFe_3CoSb_{12}$ are 77, 70, and 69 cm^{-1}, respectively [39–43].

The Raman spectra of the F_g^1 mode are demonstrated in Fig. 3(a). It can be seen that the phonon frequency softens and the FWHM widens with increasing temperature. Due to the relatively large errors in fitting the FWHM, we focus on the evolution of the frequencies with temperature. The

TABLE I. Summary of the phonon-scattering parameters obtained by fitting the temperature dependence of the frequencies of F_g^1 and F_g^2 modes through the Klemens-Hart-Aggarwal-Lax model.

Mode	ω_0 (cm^{-1})	A ($\times 10^{-3}$ cm^{-1})	B ($\times 10^{-5}$ cm^{-1})
F_g^1	81.50±0.03	–4.67±0.56	–5.56±0.32
F_g^2	106.98±0.02	–12.45±0.32	0

temperature dependence of the phonon frequencies is fitted by the Klemens-Hart-Aggarwal-Lax model [54,55]. The γ value for the F_g^1 mode is 0.50 ± 0.07. The obtained results are plotted as functions of temperature in Fig. 3(c). As can be seen, the fitting curves match well with the experimental data. The contribution from the thermal expansion for the F_g^1 mode is not negligible but low. Both three- and four-phonon scattering processes are involved in the vibration of the F_g^1 mode and contribute to the anharmonic nature of the phonons. The fitting parameters are listed in Table I. At temperatures above 300 K, the curve deviates from the three-phonon scattering process curve and is consistent with the four-phonon scattering process curve. These results suggest a contribution from four-phonon scattering processes.

The F_g^2 phonon mode is next to the F_g^1 mode and is also the optic branch close to the second Einstein mode in Yb-filled skutterudite. The assignment of the F_g^2 mode is illustrated in Fig. 4(b). The phonon mode is also due to the vibration of the Sb atoms, which is the short side in-plane shear of the Sb_4 ring, following previous studies [21]. As for this vibrational mode, the Raman frequency corresponding to the parent skutterudite $CoSb_3$ is 101 cm^{-1} at 300 K, and the frequencies corresponding to the filled skutterudites $LaFe_3CoSb_{12}$, $CeFe_3CoSb_{12}$, and $LaCeFe_3CoSb_{12}$ are 97, 89, and 81 cm^{-1}, respectively [39–43].

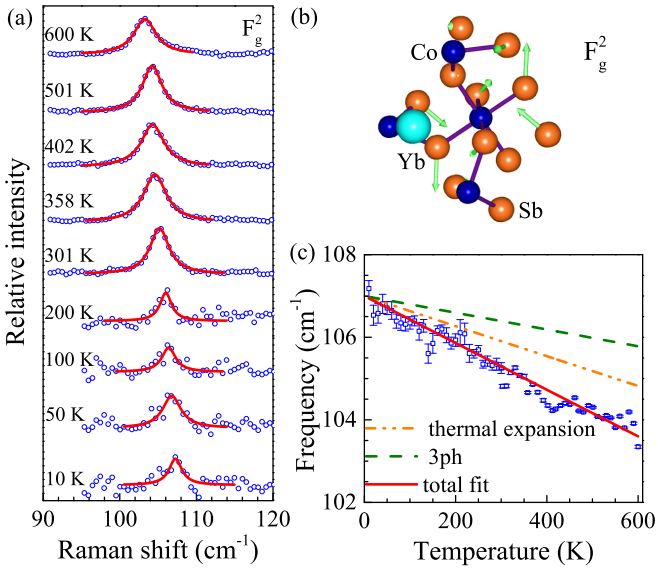

FIG. 4. (a) Raman spectra of the F_g^2 mode at various temperatures from 10 to 600 K. The open circles are the experimental data points, and the curves are the fitting results by using a single Lorentzian function for the mode. (b) The vibration directions of the atoms for the F_g^2 mode. (c) Temperature dependence of the frequency of the F_g^2 mode. The red-solid line gives the theoretical fit using the three-phonon scattering process and thermal expansion. The dashed lines represent the three-phonon and thermal expansion contributions, respectively.

The Raman spectra of the F_g^2 mode are demonstrated in Fig. 4(a). As the temperature increases, the phonon frequency monotonically shifts towards lower frequencies, and the FWHM becomes broader. However, the fit to the FWHM has relatively large errors, so our focus remains on examining the evolution of the frequency with temperature utilizing the Klemens-Hart-Aggarwal-Lax model. The γ value for the F_g^2 mode is 1.40 ± 0.12. The obtained results are plotted as functions of temperature in Fig. 4(c). As can be seen in Fig. 4(c), the fitting curve is in good agreement with the experimental data. The contribution from the thermal expansion for the F_g^2 mode becomes important. The anharmonic nature of the F_g^2 mode is mainly attributed to the three-phonon scattering process. The fitting parameters for this mode are presented in Table I.

The above analysis gives experimental evidence for the cubic and quartic anharmonicity in the phonon scattering processes. The cubic anharmonic parameters were obtained from the F_g^2 mode, indicating the cubic anharmonic nature of the phonon vibrational modes. For the F_g^1 phonon mode, the quartic anharmonicity parameter is relatively high, suggesting a quartic anharmonicity of the phonon vibrations.

In many thermoelectric materials with low lattice thermal conductivity, low-frequency phonons are the dominant heat carriers [21,22]. The scattering mechanism of low-frequency phonons is a vital factor in reducing lattice thermal conductivity. A previous study has predicted quartic anharmonicity of acoustic phonons in filled skutterudites by a four-phonon Fermi resonance scattering mechanism [22].

Therefore we need information on the scattering mechanism of low-frequency phonons in Yb-filled skutterudites. However, Raman spectra provide phonon vibration information on the relatively high-frequency optic-phonon modes. Therefore, to further investigate the phonon-scattering mechanism in Yb-filled skutterudites, we have calculated the phonon vibrational properties involving the third- and fourth-order anharmonic scattering processes. We have focused on the weighted phase space and scattering rates in the scattering process.

D. Weighted phase space and scattering rates

The weighted phase space is a direct measure of the number of scattering processes available for each phonon and depends only on the dispersion of the phonons. Therefore, weighted phase space is essential to understand the anharmonicity of phonon scattering. The weighted phase space as a function of frequency at temperatures of 10, 300, and 600 K are shown in Figs. 5(a)–5(c), respectively. At 10 K the weighted phase space for three- and four-phonon scattering is small and dominated by three-phonon scattering. Above 300 K, the weighted phase space increases significantly with increasing temperature. The weighted phase space of four-phonon scattering becomes increasingly

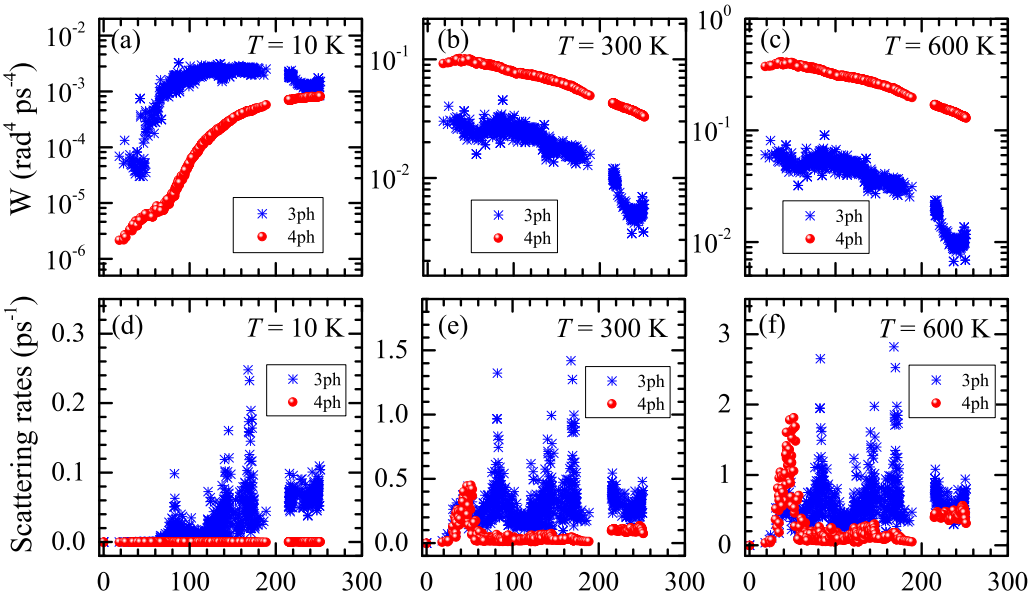

FIG. 5. Calculated phonon dynamics of the three- (blue stars) and four-phonon (red sphere) scattering processes of $YbCo_4Sb_{12}$. [(a)–(c)] The weighted phase space as a function of frequency at temperatures of 10, 300, and 600 K, respectively. [(d)–(f)] The phonon-scattering rates as a function of frequency at temperatures of 10, 300, and 600 K, respectively.

pronounced and dominates the scattering processes in Yb-filled skutterudites.

The phonon-scattering rates as a function of frequency at temperatures of 10, 300, and 600 K are shown in Figs. 5(d)–5(f), respectively. The results are similar to those for the weighted phase space. At 10 K the scattering rates are small and the three-phonon scattering rate is significantly larger than the four-phonon scattering rate. As the temperature increases, the scattering rates of the three- and four-phonon processes gradually increase and show an obvious increase above 300 K, consistent with the decrease of the lattice thermal conductivity with temperature in Fig. 1(c). A peak of the four-phonon scattering rates appears at 46 cm^{-1} in the low-frequency region, which is close to the first Einstein mode derived from the vibrations of the Yb atom. The three-phonon scattering rates have several peaks at relatively high frequencies, the lowest of which is around 80 cm^{-1}.

Above 300 K, the four-phonon scattering process contributes more and more to the phonon-scattering rate as the temperature increases. Additionally, the frequency range of the peak in the four-phonon scattering rate covers the acoustic-phonon mode and the low-frequency optic-phonon mode corresponding to the Yb-filled atoms.

To understand which phonon vibrational modes are involved in the four-phonon scattering process, we calculate the contribution of all allowed scattering channels to the four-phonon scattering process at different temperatures in $YbCo_4Sb_{12}$.

E. Four-phonon scattering process

Figure 6 shows the contribution to the four-phonon scattering process from all allowed scattering channels as a function of frequency for $YbCo_4Sb_{12}$ at temperatures of 10, 300, and 600 K, respectively. The four-phonon weighted phase space of the phonon modes at temperatures of 10, 300, and 600 K are shown in Figs. 6(a)–6(c), respectively. The four-phonon scattering processes include splitting (- -), redistribution (+ -), and combination (+ +) [24]. The splitting process is the splitting of one phonon into three phonons. The redistribution process involves one phonon absorbing another and decaying into two phonons. The combination process involves one phonon absorbing two phonons and producing one phonon.

At 10 K the weighted phase space of the four-phonon scattering is still low and dominated by the splitting process. With increasing temperature, the weighted phase space exhibits a sharp increase. Above 300 K the weighted phase space of the four-phonon scattering increases by several orders of magnitude compared to the value at 10 K. From 300 to 600 K the redistribution process dominates the low-frequency four-phonon scattering process. The splitting process at low frequencies is suppressed due to the relatively strong redistribution processes.

Notably, the weighted phase space of the four-phonon scattering shows a peak near the low frequency of 46 cm^{-1}. This peak is consistent with the peak position in the four-phonon scattering rates in Figs. 5(d)–5(f). To further investigate the origin of the peak in the weighted phase space of four-phonon scattering, we focus on the different four-phonon scattering channels and their relevance to the characteristics of the phonon dispersion.

The four-phonon scattering rates of the phonon modes at temperatures of 10, 300, and 600 K are shown in Figs. 6(d)–6(f), respectively. At 10 K the four-phonon scattering rate is small and dominated by the contribution of the optic-phonon modes generated by the Sb atoms. A peak in the four-phonon scattering rate occurs at low frequencies. The peak value increases by several orders of magnitude at 300 K and continues to increase with increasing temperature. As can be seen from

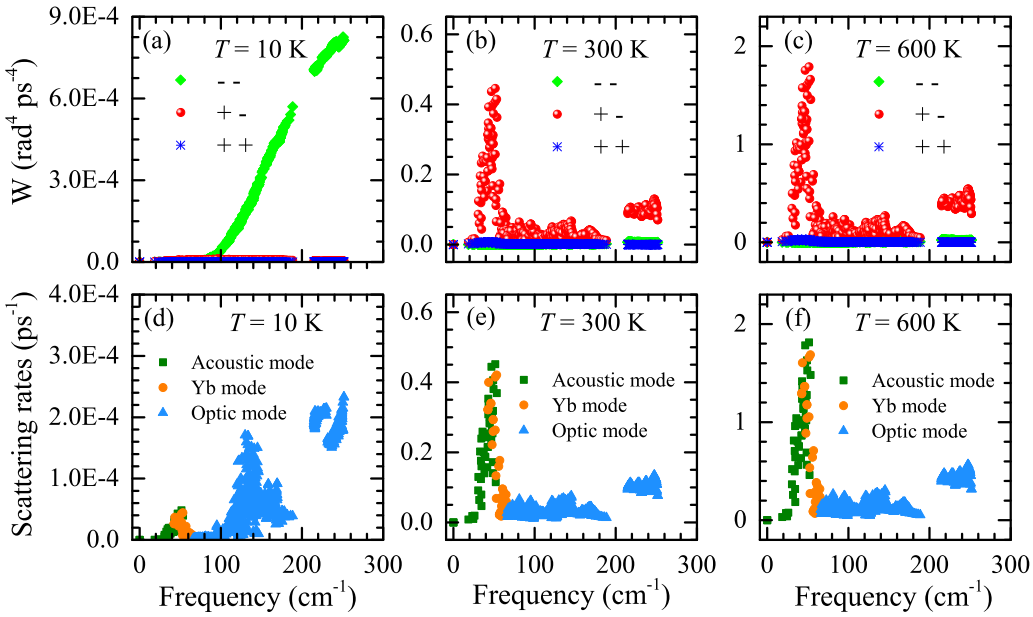

FIG. 6. Contribution to the four-phonon scattering process from all allowed scattering channels as a function of frequency for $YbCo_4Sb_{12}$ at temperatures of 10, 300, and 600 K, respectively. [(a)–(c)] The four-phonon weighted phase space of the phonon modes at temperatures of 10, 300, and 600 K, respectively. [(d)–(f)] The four-phonon scattering rates of the phonon modes at temperatures of 10, 300, and 600 K, respectively.

Figs. 6(e)–6(f), the peak frequency of the four-phonon scattering rate covers the interval of the acoustic-phonon mode and Yb-phonon mode. Hence, acoustic phonons and Yb atom vibrations dominate the four-phonon scattering process.

Previous studies have shown the avoided crossing between the flat Yb-phonon mode and longitudinal acoustic-phonon mode [21]. In addition, the transverse acoustic branch in Yb-filled skutterudite exhibits a unique flat energy dispersion in the Brillouin zone [21,22]. As described in the literature [22], the unique flat energy dispersion and the quartic anharmonic interaction result in the four-phonon Fermi resonances and significantly increase the probability of four-phonon interaction scattering of the acoustic branch phonons, ultimately leading to a suppression of the lattice thermal conductivity. This model has been demonstrated to work well for materials with flat energy dispersion, such as $AgCrSe_2$, copper halogen, SnSe, and $PbTiO_3$ [22]. Based on the four-phonon weighted phase space and scattering rate calculations, we speculate that Yb filling affects the acoustic phonons.

In this study, the redistribution process dominates the four-phonon scattering process at high temperatures. As depicted in Fig. 1(b), during the redistribution of the four-phonon scattering process, the optic phonon can absorb one phonon and decay into two phonons. Following energy and quasimomentum conservation, phonon decay can generally occur through down-conversion or up-conversion into various frequency combinations, depending on the PDOS [56]. Due to the flat characteristic of the Yb mode and that the acoustic-phonon mode and their frequencies are near, the PDOS exhibits peaks around 42 cm^{-1} [21]. The high density of states provides the basis for Fermi resonance scattering [58]. The three-phonon scattering process is thus limited according to the selection rules [59]. The four-phonon scattering rate is unaffected by the selection rules, and any two phonons of the same frequency can combine to form two new phonons [59]. Thus a possible redistribution process is that one optic phonon from the Yb vibrational mode absorbs one acoustic phonon and decays into two acoustic phonons. Under this circumstance, the optic phonons produced by the Yb-filled atoms and the acoustic phonons undergo four-phonon Fermi resonance scattering. It is also possible for one acoustic phonon to combine with another to create two acoustic phonons, or for one optic phonon from the vibration of Yb atoms to combine with another to create two optic phonons [22,27,28].

Our previous studies have shown that the hybridization of Yb atoms with the parent framework leads to strong anharmonicity in filled skutterudites [21]. The F_g^1 mode is associated with both three- and four-phonon scattering processes. As shown in Figs. 6(a)–6(c), during the frequency range of the F_g^1 mode, the distribution process remains prevalent over the four-phonon scattering process. The PDOS of Yb-filled $CoSb_3$ skutterudite shows peaks at around 80 cm^{-1} [21], Hence we cautiously speculate that the three-phonon process associated with the F_g^1 mode could involve the decay of one optic phonon from the Sb atom into two low-frequency phonons. Furthermore, the four-phonon process may occur when an optic phonon from the Sb atom absorbs another from the Yb atom and decays into two low-frequency optic phonons. A possible scenario for the three-phonon process in the F_g^2 mode is the decay of one optic phonon from the Sb atom into two low-frequency optic phonons. Of course, there are many other possibilities for the phonon-scattering processes.

Therefore the microscopic mechanism of phonon scattering in Yb-filled $CoSb_3$ skutterudite is closely related to the hybridization between the Yb-filled atoms and the parent. The cubic and quartic anharmonicity are involved in the phonon-scattering processes. Four-phonon Fermi resonance scattering

presumably occurs between the Yb-filled atom and the parent atom, as evidenced by the four-phonon peak at low frequencies. The Yb-filled atom undergoes the three- and four-phonon scattering processes with the optic phonons of Sb atoms. At high temperatures, four-phonon scattering dominates the scattering process at low frequencies. The Fermi resonances among low-frequency phonons provide strong four-phonon scattering. Such low-frequency phonons account for the low lattice thermal conductivity in many efficient thermoelectric materials [22]. Therefore phonon anharmonicity, especially quartic anharmonicity, is responsible for the low lattice thermal conductivity in Yb-filled skutterudites.

IV. CONCLUSIONS

In summary, the phonon-scattering microscopic mechanism in Yb-filled skutterudite has been investigated by combining temperature-dependent Raman-scattering measurements and first-principles calculations. We have verified the anharmonicity of phonon vibrations in Yb-filled skutterudites by studying the Raman spectra over a temperature range from 10 to 600 K. The phonons have strong temperature dependence. Based on the temperature-dependent phonon frequencies, we find that the phonon modes F_g^1 and F_g^2 exhibit strong quartic and cubic anharmonicity, respectively. The calculated weighted phase space and scattering rates of the three- and four-phonon scattering processes fully support the phonon anharmonicity obtained from Raman-scattering measurements, providing detailed information about the phonon-scattering processes. Moreover, it is worth noting that four-phonon scattering dominates the phonon-scattering processes at low frequencies. Fermi resonances among low-frequency phonons provide strong four-phonon scattering, and thus the lattice thermal conductivity is effectively suppressed at high temperatures. Our study reveals the important role of higher-order anharmonicity in phonon thermal transport and provides a comprehensive understanding of the microscopic mechanisms responsible for the low lattice thermal conductivity in Yb-filled skutterudites.

ACKNOWLEDGMENTS

We thank Prof. X. Shi and Prof. L. D. Chen for providing samples and valuable discussions. We are grateful for the helpful guidance from Prof. Xiao Qun Wang from Shanghai Jiaotong University. This work is funded through the Shenzhen Science and Technology Program (Grant No. KQTD20200820113045081) and the Basic Research Program of Shenzhen (Grant No. JCYJ20200109112810241) at HIT.

[1] G. A. Slack, in *CRC Handbook of Thermoelectrics*, edited by D. M. Rowe (CRC, Boca Raton, FL, 1995).

[2] G. J. Snyder and E. S. Toberer, Complex thermoelectric materials, Nat. Mater. **7**, 105 (2008).

[3] B. Poudel, Q. Hao, Y. Ma, Y. C. Lan, A. Minnich, B. Yu, X. Yan, D. Z. Wang, A. Muto, D. Vashaee, X. Y. Chen, J. M. Liu, M. S. Dresselhaus, G. Chen, and Z. F. Ren, High-thermoelectric performance of nanostructured bismuth antimony telluride bulk alloys, Science **320**, 634 (2008).

[4] K. Biswas, J. Q. He, I. D. Blum, C. I. Wu, T. P. Hogan, D. N. Seidman, V. P. Dravid, and M. G. Kanatzidis, High-performance bulk thermoelectrics with all-scale hierarchical architectures, Nature (London) **489**, 414 (2012).

[5] J. Ma, O. Delaire, A. F. May, C. E. Carlton, M. A. McGuire, L. H. VanBebber, D. L. Abernathy, G. Ehlers, T. Hong, A. Huq, W. Tian, V. M. Keppens, Y. Shao-Horn, and B. C. Sales, Glass-like phonon scattering from a spontaneous nanostructure in $AgSbTe_2$, Nat. Nanotechnol. **8**, 445 (2013).

[6] G. P. Meisner, D. T. Morelli, S. Hu, J. Yang, and C. Uher, Structure and lattice thermal conductivity of fractionally filled skutterudites: Solid solutions of fully filled and unfilled end members, Phys. Rev. Lett. **80**, 3551 (1998).

[7] T. Dahal, Q. Jie, G. Joshi, S. Chen, C. F. Guo, Y. C. Lan, and Z. F. Ren, Thermoelectric property enhancement in Yb-doped *n*-type skutterudites $Yb_xCo_4Sb_{12}$, Acta Mater. **75**, 316 (2014).

[8] S. Y. Wang, J. R Salvador, J. Yang, P. Wei, B. Duan, and J. H. Yang, High-performance *n*-type $Yb_xCo_4Sb_{12}$: From partially filled skutterudites towards composite thermoelectrics, NPG Asia Mater. **8**, e285 (2016).

[9] X. Shi, S. Q. Bai, L. L. Xi, J. Yang, W. Q. Zhang, L. D. Chen, and J. H. Yang, Realization of high thermoelectric performance in *n*-type partially filled skutterudites, J. Mater. Res. **26**, 1745 (2011).

[10] X. Shi, J. Yang, J. R. Salvador, M. F. Chi, J. Y. Cho, H. Wang, S. Q. Bai, J. H. Yang, W. Q. Zhang, and L. D. Chen, Multiple-filled skutterudites: High thermoelectric figure of merit through separately optimizing electrical and thermal transports, J. Am. Chem. Soc. **133**, 7837 (2011).

[11] V. Keppens, D. Mandrus, B. C. Sales, B. C. Chakoumakos, P. Dai, R. Coldea, M. B. Maple, D. A. Gajewski, E. J. Freeman, and S. Bennington, Localized vibrational modes in metallic solids, Nature (London) **395**, 876 (1998).

[12] G. S. Nolas, D. T. Morelli, and T. M. Tritt, Skutterudites: A phonon-glass-electron-crystal approach to advanced thermoelectric energy conversion applications, Annu. Rev. Mater. Sci. **29**, 89 (1999).

[13] M. M. Koza, M. R. Johnson, R. Viennois, H. Mutka, L. Girard, and D. Ravot, Breakdown of phonon glass paradigm in La- and Ce-filled Fe_4Sb_{12} skutterudites, Nat. Mater. **7**, 805 (2008).

[14] I. K. Dimitrov, M. E. Manley, S. M. Shapiro, J. Yang, W. Zhang, L. D. Chen, Q. Jie, G. Ehlers, A. Podlesnyak, J. Camacho, and Q. Li, Einstein modes in the phonon density of states of the single-filled skutterudite $Yb_{0.2}Co_4Sb_{12}$, Phys. Rev. B **82**, 174301 (2010).

[15] I. Sergueev, K. Glazyrin, I. Kantor, M. A. McGuire, A. I. Chumakov, B. Klobes, B. C. Sales, and R. P. Hermann, Quenching rattling modes in skutterudites with pressure, Phys. Rev. B **91**, 224304 (2015).

[16] M. Christensen, A. B. Abrahamsen, N. B. Christensen, F. Juranyi, N. H. Andersen, K. Lefmann, J. Andreasson, C. R. H.

Bahl, and B. B. Iversen, Avoided crossing of rattler modes in thermoelectric materials, Nat. Mater. **7**, 811 (2008).

[17] W. Li and N. Mingo, Ultralow lattice thermal conductivity of the fully filled skutterudite $YbFe_4Sb_{12}$ due to the flat avoided-crossing filler modes, Phys. Rev. B **91**, 144304 (2015).

[18] M. M. Koza, M. Boehm, E. Sischka, W. Schnelle, H. Mutka, and A. Leithe-Jasper, Low-energy phonon dispersion in $LaFe_4Sb_{12}$, Phys. Rev. B **91**, 014305 (2015).

[19] M. M. Koza, A. Leithe-Jasper, H. Rosner, W. Schnelle, H. Mutka, M. R. Johnson, M. Krisch, L. Capogna, and Y. Grin, Vibrational dynamics of the filled skutterudites $M_{1-x}Fe_4Sb_{12}$ (M=Ca, Sr, Ba, and Yb): Temperature response, dispersion relation, and material properties, Phys. Rev. B **84**, 014306 (2011).

[20] C. Chang and L. D. Zhao, Anharmonicity and low thermal conductivity in thermoelectrics, Mater. Today Phys. **4**, 50 (2018).

[21] H. J. Pang, L. C. Chen, H. Yu, P. F. Qiu, G. H. Zhong, Q. Peng, and X. J. Chen, Hybridization-driven strong anharmonicity in Yb-filled skutterudites, Phys. Rev. B **105**, 094115 (2022).

[22] L. Xie, J. H. Feng, R. Li, and J. Q. He, First-principles study of anharmonic lattice dynamics in low thermal conductivity $AgCrSe_3$: Evidence for a large resonant four-phonon scattering, Phys. Rev. Lett. **125**, 245901 (2020).

[23] J. Z. Zheng, D. L. Shi, S. J. Liu, Y. W. Yang, C. J. Lin, Z. Chang, R. Q. Guo, and B. L. Huang, Effects of high-order anharmonicity on anomalous lattice dynamics and thermal transport in fully filled skutterudite $YbFe_4Sb_{12}$, Phys. Rev. Mater. **6**, 093801 (2022).

[24] T. L. Feng and X. L. Ruan, Quantum mechanical prediction of four-phonon scattering rates and reduced thermal conductivity of solids, Phys. Rev. B **93**, 045202 (2016).

[25] T. L. Feng, L. Lindsay, and X. L. Ruan, Four-phonon scattering significantly reduces intrinsic thermal conductivity of solids, Phys. Rev. B **96**, 161201(R) (2017).

[26] T. L. Feng, X. L. Yang, and X. L. Ruan, Phonon anharmonic frequency shift induced by four-phonon scattering calculated from first principles, J. Appl. Phys. **124**, 145101 (2018)

[27] X. L. Yang, T. L. Feng, J. Li, and X. L. Ruan, Stronger role of four-phonon scattering than three-phonon scattering in thermal conductivity of III-V semiconductors at room temperature, Phys. Rev. B **100**, 245203 (2019).

[28] X. L. Yang, T. L. Feng, J. S. Kang, Y. J. Hu, J. Li, and X. L. Ruan, Observation of strong higher-order lattice anharmonicity in Raman and infrared spectra, Phys. Rev. B **101**, 161202(R) (2020).

[29] Z. R. Han, X. L. Yang, W. Li, T. L. Feng, and X. L. Ruan, FourPhonon: An extension module to ShengBTE for computing four-phonon scattering rates and thermal conductivity, Comput. Phys. Commun. **270**, 108179 (2022).

[30] Y. Zhou, Z. Y. Dong, W. P. Hsieh, A. F. Goncharov, and X. J. Chen, Thermal conductivity of materials under pressure, Nat. Rev. Phys. **4**, 319 (2022).

[31] C. W. Li, J. Hong, A. F. May, D. Bansal, S. Chi, T. Hong, G. Ehlers, and O. Delaire, Orbitally driven giant phonon anharmonicity in SnSe, Nat. Phys. **11**, 1063 (2015).

[32] X. J. Chen, V. V. Struzhkin, S. Kung, H. K. Mao, R. J. Hemley, and A. N. Christensen, Pressure-induced phonon frequency shifts in transition-metal nitrides, Phys. Rev. B **70**, 014501 (2004).

[33] L. C. Chen, Z. Y. Cao, H. Yu, B. B. Jiang, L. Su, X. Shi, L. D. Chen, and X. J. Chen, Phonon anharmonicity in thermoelectric palladium sulfide by Raman spectroscopy, Appl. Phys. Lett. **113**, 022105 (2018).

[34] Z. Y. Cao and X. J. Chen, Phonon scattering processes in molybdenum disulfide, Appl. Phys. Lett. **114**, 052102 (2019).

[35] Y. K. Peng, Z. Y. Cao, L. C. Chen, N. Dai, Y. Sun, and X. J. Chen, Phonon anharmonicity of tungsten disulfide, J. Phys. Chem. C **123**, 25509 (2019).

[36] Z. Y. Dong, Y. Zhou, X. Q. Chen, W. J. Li, Z. Y. Cao, C. Luo, G. H. Zhong, Q. Peng, X. Wu, and X. J. Chen, Effect of low-frequency optical phonons on the thermal conductivity of 2H molybdenum disulfide, Phys. Rev. B **105**, 184301 (2022).

[37] H. Yu, L. C. Chen, H. J. Pang, P. F. Qiu, Q. Peng, and X. J. Chen, Temperature-dependent phonon anharmonicity and thermal transport in $CuInTe_2$, Phys. Rev. B **105**, 245204 (2022).

[38] F. X. Bai, H. Yu, D. Peng, H. J. Pang, L. Yu, L. C. Chen, J. Mao, Q. Zhang, and X. J. Chen, Strong acoustic-optical phonon coupling in high-performance thermoelectric material $Bi_{0.5}Sb_{1.5}Te_3$, Mater. Today Phys. **37**, 101200 (2023).

[39] G. S. Nolas and G. A. Slack, Raman scattering study of antimony based skutterudites, J. Appl. Phys. **79**, 2622 (1996).

[40] G. S. Nolas and C. A. Kendziora, Raman spectroscopy investigation of lanthanide-filled and unfilled skutterudites, Phys. Rev. B **59**, 6189 (1999).

[41] G. S. Nolas, C. A. Kendziora, and H. Takizawa, Polarized Raman-scattering study of Ge and Sn-filled $CoSb_3$, J. Appl. Phys. **94**, 7440 (2003).

[42] L. X. Li, H. Liu, J. Y. Wang, X. B. Hu, S. R. Zhao, H. D. Jiang, Q. J. Huang, H. H. Wang, and Z. F. Li, Raman spectroscopy investigation of partially filled skutterudite, Chem. Phys. Lett. **347**, 373 (2001).

[43] R. Viennois, T. Kume, M. Komura, L. Girard, A. Haidoux, J. Rouquette, and M. M. Koza, Raman-scattering experiments on unfilled skutterudite $CoSb_3$ under high pressure and high temperature, J. Phys. Chem. C **124**, 23004 (2020).

[44] E. Liarokapis, E. Anastassakis, and G. A. Kourouklis, Raman study of phonon anharmonicity in LaF_3, Phys. Rev. B **32**, 8346 (1985).

[45] Y. L. Li, P. F. Qiu, Z. Xiong, J. K. Chen, R. Nunna, X. Shi, and L. D. Chen, Electrical and thermal transport properties of $Yb_xCo_4Sb_{12}$ filled skutterudites with ultrahigh carrier concentrations, AIP Adv. **5**, 117239 (2015).

[46] J. P. Perdew, K. Burke, and M. Ernzerhof, Generalized gradient approximation made simple, Phys. Rev. Lett. **77**, 3865 (1996).

[47] G. Kresse and J. Joubert, From ultrasoft pseudopotentials to the projector augmented-wave method, Phys. Rev. B **59**, 1758 (1999).

[48] G. Kresse and J. Furthmüller, Efficient iterative schemes for ab initio total-energy calculations using a plane-wave basis set, Phys. Rev. B **54**, 11169 (1996).

[49] G. Rogl, L. Zhang, P. Rogl, A. Grytsiv, M. Falmbigl, D. Rajs, M. Kriegisch, H. Müller, E. Bauer, J. Koppensteiner, W. Schranz, M. Zehetbauer, Z. Henkie, and M. B. Maple, Thermal expansion of skutterudites, J. Appl. Phys. **107**, 043507 (2010).

[50] A. Togo, F. Oba, and I. Tanaka, First-principles calculations of the ferroelastic transition between rutile-type and $CaCl_2$-type SiO_2 at high pressures, Phys. Rev. B **78**, 134106 (2008).

[51] W. Li, J. Carrete, N. A. Katcho, and N. Mingo, ShengBTE: A solver of the Boltzmann transport equation for phonons, Comput. Phys. Commun. **185**, 1747 (2014).

[52] Y. Xiao, H. J. Wu, J. Cui, D. Y. Wang, L. W. Fu, Y. Zhang, Y. Chen, J. Q. He, S. J. Pennycook, and L. D. Zhao, Realizing high performance *n*-type PbTe by synergistically optimizing effective mass and carrier mobility and suppressing bipolar thermal conductivity, Energy Environ. Sci. **11**, 2486 (2018).

[53] X. Shi, L. Chen, and C. Uher, Recent advances in high-performance bulk thermoelectric materials, Int. Mater. Rev. **61**, 379 (2016).

[54] P. G. Klemens, Anharmonic decay of optic phonons, Phys. Rev. **148**, 845 (1966).

[55] M. Balkanski, R. F. Wallis, and E. Haro, Anharmonic effects in light scattering due to optical phonons in silicon, Phys. Rev. B **28**, 1928 (1983).

[56] F. Liu, P. Parajuli, R. Rao, P. C. Wei, A. Karunarathne, S. Bhattacharya, R. Podila, J. He, B. Maruyama, G. Priyadarshan, J. R. Gladden, Y. Y. Chen, and A. M. Rao, Phonon anharmonicity in single-crystalline SnSe, Phys. Rev. B **98**, 224309 (2018).

[57] Z. Y. Zhao, J. Elwood, and M. A. Carpenter, Phonon anharmonicity of PdO studied by Raman spectrometry, J. Phys. Chem. C **119**, 23094 (2015).

[58] G. Kanellis, W. Kress, and H. Bilz, Fermi resonance in the phonon spectra of copper halides, Phys. Rev. Lett. **56**, 938 (1986).

[59] N. K. Ravichandran and D. Broido, Phonon-phonon interactions in strongly bonded solids: Selection rules and higher-order processes, Phys. Rev. X **10**, 021063 (2020).